PHYSICAL REVIEW E **76**, 040401(R) (2007)

Nematic and almost-tetratic phases of colloidal rectangles

Kun Zhao,[1] Christopher Harrison,[2] David Huse,[1] W. B. Russel,[3] and P. M. Chaikin[4,*]
[1]*Department of Physics, Princeton University, Princeton, New Jersey 08544, USA*
[2]*Schlumberger-Doll Research Center, Ridgefield, Connecticut 06877, USA*
[3]*Department of Chemical Engineering, Princeton University, Princeton, New Jersey 08544, USA*
[4]*Center for Soft Condensed Matter Research, Department of Physics, New York University, New York, New York 10003, USA*
(Received 9 April 2006; published 11 October 2007)

Nonspherical colloids can exhibit liquid-crystalline phases with different degrees of broken orientational and translational symmetry. Here we investigate hard rectangles consisting of photolithographically prepared disks standing on edge. We observe a conventional Kosterlitz-Thouless transition from isotropic to nematic with almost smectic behavior at high density. But just on the isotropic side of the isotropic to nematic transition we observe an unusual regime where short-range tetratic correlations dominate over nematic correlations. This occurs due to the proliferation of Ising-like $\pi/2$ grain boundaries that disrupt nematic order, but preserve tetratic correlations, at lengths shorter than the spacing between free disclinations.

DOI: 10.1103/PhysRevE.76.040401 PACS number(s): 82.70.Dd, 64.70.Md

In hard-particle systems, shape, packing, and associated excluded-volume effects determine the entropy and the phase diagram. The most well-known examples are the isotropic-nematic transition of rodlike systems [1] and the crystallization of hard spheres [2]. In three dimensions both transitions are typically first order. In two dimensions (2D) they can also be second order and involve the unbinding of topological defects, and there can be several hierarchical steps of broken symmetry in approaching the ordered state. There have been several theoretical and computational studies of various disk and rodlike systems over the past decade [3–10]. In 3D disk systems, aside from the nematic, smectic, and columnar order expected from the basic symmetry of the particles, there are also indications of intermediate cubatic phases [4]. Similarly for 2D rodlike systems there has been interest in the possibility of a tetratic phase with $\langle\cos(4\theta)\rangle$ order along with the more common $\langle\cos(2\theta)\rangle$ nematic order [5–8]. Recent papers suggest that the existence of a tetratic phase is very sensitive to details of the rodlike shape [9,10]. The simulations also suggest a phase diagram with two possible scenarios: a direct transition from isotropic liquid to crystal with a first-order transition or a transition from isotropic to a liquid-crystal phase (nematic or tetratic) via a Kosterlitz-Thouless (KT) transition and then a transition to a crystal (smectic) phase.

The experiments we present here indicate a different scenario with order evolving from isotropic to tetratic to nematic to smectic as the concentration/volume fraction is increased. There appears only one true phase transition, a KT transition from isotropic to nematic. But preceding the nematic transition, there are strong tetratic correlations which dominate the observed behavior. At high density the short-range smectic order also persists for many particle lengths. Nematic→tetratic→isotropic melting would be interesting. From nematic to tetratic one would expect an Ising-like transition with proliferation of $\pi/2$ grain boundaries separating horizontal and vertically aligned nematic regions. At lower densities unbinding of $\pi/2$ disclination pairs would lead to a KT transition from tetratic to isotropic. We believe our observations are a remnant of this type of combined Ising-KT transition. Such combined continuous-discrete symmetry breaking has been studied in the context of the frustrated x-y model. [11].

There are several novel techniques employed in the fabrication of the samples and in obtaining the phase diagram of this system. The colloidal particles are platelike disks of diameter $d=5.3$ μm and thickness $t=0.8$ μm made by photolithography. An ac electric field is used to orient the disks so that they stand "on edge." Their gravitational height is $h_g=0.12$ μm ($h_g=\Delta\rho Vg/k_BT$)$<d$, so they form a monolayer. The cell is tilted at an angle $\sim 2°$ with respect to the horizontal so that in equilibrium gravity and osmotic pressure produce a concentration profile which allows observation of the complete phase diagram with a single sample of dimensions 1.5×1.5 mm.

Photolithography can produce $\sim 10^8$–10^{10}-μm-scale particles [12] of arbitrary two-dimensional shape on a commercial 3–6-in. wafer. Care must be taken to use compatible layers that do not interfere with (i.e., dissolve) each other. Here we use spin coating, a hexamethyldisilazine wetting layer, an AZP 4110 photoresist (Hoescht) sacrificial layer (to allow liftoff), a PMMA (molecular weight 495 000) colloidal layer, and an AZP 4110 photoresist top layer for exposure. A Karl Suss MA6 mask aligner is used in "hard-contact mode" operating at 365 nm through a chromium-coated laser-scribed mask (Adtek Photomask) on a 4-in. quartz substrate patterned with a square lattice (15 μm periodicity) of 5-μm metal circles. The top layer is developed and samples are then etched with a PlasmaTherm 790 reactive ion etcher using an oxygen plasma. Figure 1(a) shows a SEM of 4.5-μm-diam and 0.8-μm-thick disks which are similar to the 5.3 μm$\times$0.8 μm disks used in this study. The polydispersity in the diameter of the disks is 5.5%. The colloidal disks are stable in water with a negative surface charge density $\sim 1e/200$ nm^2 determined by electrophoresis. The Debye length is 0.03 μm in a solution with ionic strength $1.5\times 10^{-4}M$.

*chaikin@physics.nyu.edu

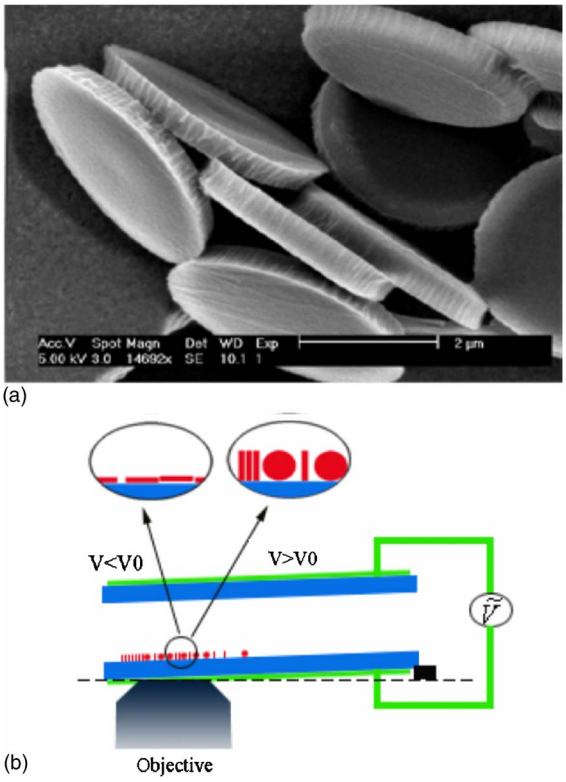

FIG. 1. (Color online) (a) Scanning electron micrograph of photolithographically prepared 4.5-μm-diam, 0.8-μm-thick PMMA disks. (b) Schematic of the experimental setup. Particles settle to a monolayer on the bottom of the sample chamber and stand on edge in the applied field. Dashed line indicates the horizontal plane.

Figure 1(b) is a schematic of our sample cell. Contactless electrodes on the outside of the cell produce an ac field, 220 kHz, 52 V/cm rms at the particles. The PMMA disks have both shape and molecular dielectric anisotropy $\Delta\varepsilon=\varepsilon_{\parallel}-\varepsilon_{\perp}$. The energy, U of particles of volume v_p and density mismatch $\Delta\rho$, in a vertical electric field E, with an angle θ of the disk plane to the horizontal is $\frac{U}{v_p}=-\frac{\Delta\varepsilon E^2}{2}(\sin\theta)^2+\frac{\Delta\rho g d}{2}\sin\theta$, which has two stable minimum at $\theta=0$ and at $\theta=\pi/2$. The particles lie flat for $\Delta\epsilon E^2<\Delta\rho g d$ and stand on edge for $\Delta\epsilon E^2>\Delta\rho g d$. For these experiments the applied field is twice the field where disks are observed to "stand up." At this field thermal fluctuations allow for an rms tilt from vertical of $\sim 5°$ so the system is slightly different from ideal hard rods.

Figure 2(a) shows optical micrographs of the sample in the volume fraction regimes of interest. The disks standing on edge and viewed from below appear as rods and will be referred to as rods in the following. The rightmost frame shows the most ordered phase, which is nematic and close to smectic. That is, large regions of periodic, parallel, vertical, columns of stacked horizontal rods are evident. The inset shows a Fourier transform of the frame with two narrow peaks indicating the periodic density modulation. Translational order is broken both by undulations (Landau-Peierls fluctuations give a lower critical dimension of 3 for the smectic phase [13]) and dislocations. Nematic order in this phase is long range, at least longer than the picture, 100 μm $\sim$ 20 rod lengths. Note the complete lack of π disclinations in this panel. The middle figure is of most interest here. Tetratic order is discernible in the pattern of vertically and horizontally arranged rods. The leftmost frame shows the isotropic phase. Stacks of rods are still visible but so are numerous disclinations.

Orientational order is characterized by an order parameter $S_{2m}\equiv\langle\cos(2m\theta)\rangle$ and a correlation function $g_{2m}(r)\equiv\langle\cos\{2m[\theta(0)-\theta(r)]\}\rangle$, where $m=1,2,3\ldots$ corresponds to nematic, tetratic, hexatic, etc. [6]. In Fig. 2(b) we show the correlation functions associated with the micrographs of the

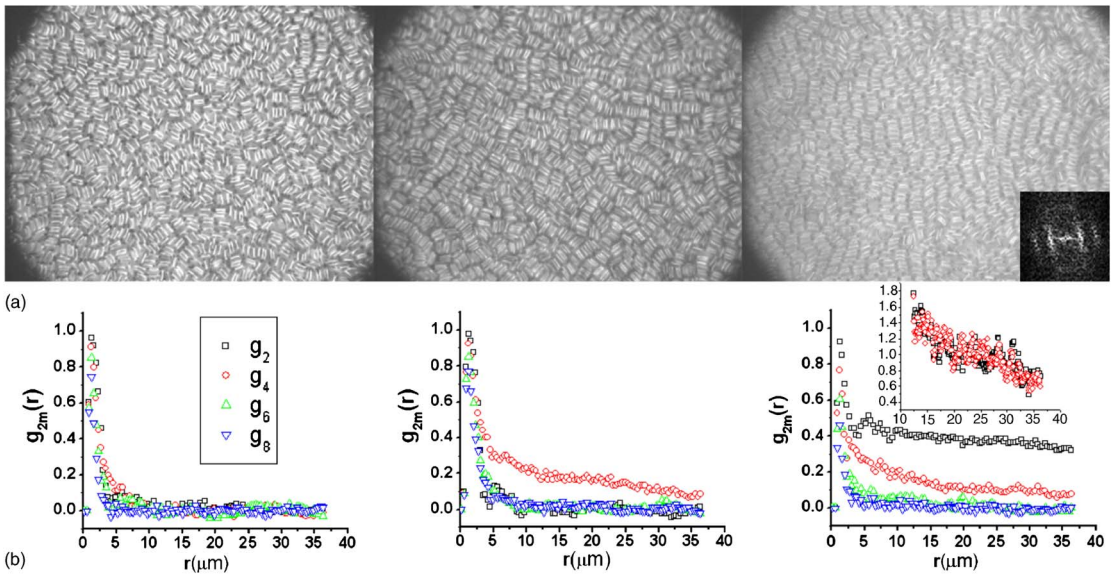

FIG. 2. (Color online) (a) Optical micrographs of the sample at 2D packing fractions of 0.50, 0.53, and 0.56 from left to right. Inset on right is Fourier transform of 0.56 image. (b) Orientational correlation functions associated with the micrographs. Square, g_2; circle g_4; up triangle, g_6; down triangle, g_8. Inset of right image shows the $[g_2(r)]^4$ and $g_4(r)$ overlay, indicating both arise from nematic order.

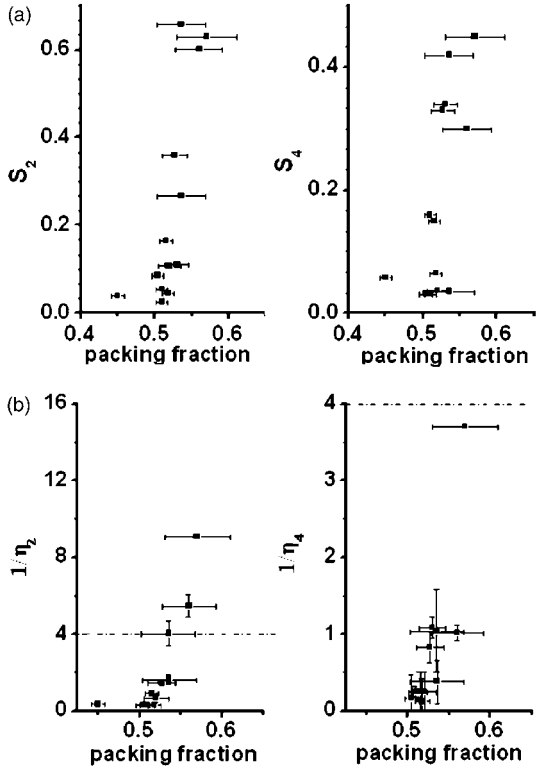

FIG. 3. (a) Nematic and tetratic order parameter and (b) nematic and tetratic decay exponent as a function of 2D packing fraction. For the nematic phase, the Franck constant has a relation with η_2: $\eta_2 = 2k_BT/\pi K$.

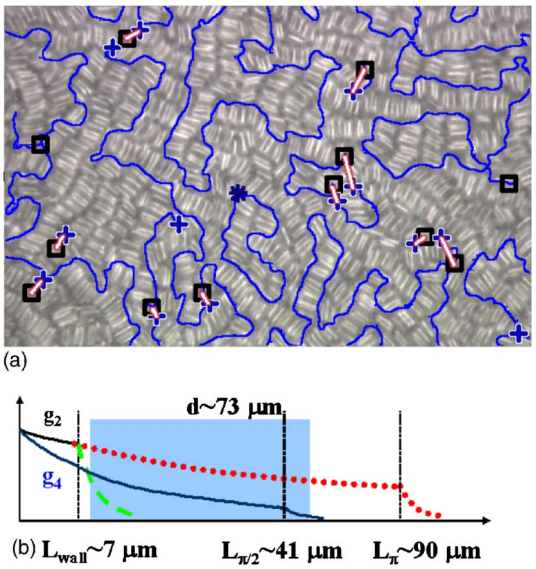

FIG. 4. (Color online) (a) Disclinations and domain walls for the almost tetratic sample. Star, plus, and square denote π, $\pi/2$, and $-\pi/2$ dislcinations, respectively. Lines (blue in color) indicate the location of walls. Bound tetratic disclinations are connected by white segments (white-red in color). The free disclinations are shown in isolated symbols. (b) Schematic of correlation functions arising from topological defects. The dotted line represents the nematic correlation function $g_2(r)$ expected from the distance between π disclinations. The solid line represents the tetratic correlation function $g_4(r)$ expected from $g_2(r)$ + the distance between $\pi/2$ disclinations. The dashed line represents $g_2(r)$ expected from the separation length of grain boundaries + the distance between π disclinations. The $\pi/2$ grain boundaries, of separation L_{wall}, destroy nematic but not tetratic correlations. Thus in our observation window $d \sim 73$ μm, g_4 dominates over g_2.

different phases. The correlation functions are calculated from an interactive data language (IDL) algorithm which locates the center and long axis of each rod. In the isotropic phase the correlation functions decay rapidly to zero on the distance scale of a rod length. In the nematic phase the decay is much slower both for g_2 and g_4. Of course, perfect order for one m will produce perfect order for all higher m and correlation for $m=1$ will induce correlation in $g_{2m>2}$. In fact, for power law decay in $g_2 \propto r^{-\eta}$ we expect power law decay $g_{2m} \propto r^{-\eta m^2}$ [6,14]. For the nematic we plot $(g_2)^4$ and g_4 together as the inset of Fig. 2(b). The strong overlap confirms that the tetratic correlations in this phase are parasitic to the nematic order. Such a simple parasitic dependence cannot, however, explain the behavior in the middle panel of Fig. 2(b) where g_4 is larger and longer ranged than g_2. This is where we might expect a tetratic phase.

Theoretically both the nematic-isotropic and tetratic-isotropic transitions are expected to be KT transitions [15] caused by unbinding of π or $\pi/2$ disclinations respectively. Associated with the unbinding is a discontinuous drop of an elastic (Franck) constant from a universal value $K = m^2 8k_BT/\pi$ to zero [13,16–18]. The elastic constant responsible for order parameter rigidity determines the range of the correlation function $g_{2m}(r) \sim ar^{-2m^2k_BT/\pi K} \sim ar^{-\eta_{2m}}$ and the decay of the average order parameter with system size, $S_{2m} \sim cN^{-k_BTm^2/2\pi K} \sim cN^{-\eta_{2m}/4}$ [6,14]. For thermodynamic stability the exponent η_{2m} must be less than $\frac{1}{4}$ for the smallest m that shows quasi-long-range order [15,16,18].

Suppose that the sequence of transitions is isotropic-tetratic-nematic. Then on increasing density the complete continuous rotational symmetry is broken in favor of a system with discrete fourfold rotations via a KT transition. The discrete fourfold tetratic symmetry would then be further broken by an Ising transition to a nematic with discrete twofold rotations. This latter transition would be mediated by the growth of horizontally and vertically aligned nematic domains and the elimination of the $\pi/2$ domain walls separating these domains.

The first test of this scenario is the value of the exponent η_4. Our measurements of g_4 never yield a value of η_4 less than 1/4. In fact, the value of η_4 in the tetraticlike region is ~1. In Fig. 3(b) we plot $1/\eta_2$ and $1/\eta_4$ as a function of the particle density or packing fraction. We see that $1/\eta_4 < 4$ and $\eta_4 > 1/4$ in the density region below the nematic phase where $1/\eta_2 > 4$ Thus with $\eta_4 > \frac{1}{4}$ we do not have a true tetratic phase. The next question is whether we have a true, stable, nematic phase. In Fig. 3 we show the nematic order parameter S_2 evaluated as an average over a 73 μm $\times$ 112 μm window along with the exponent η_2 from the dependence of S_2 on N. Here we see that S_2, the Franck

constant, and η_2^{-1} increase from near zero in the isotropic phase and that η_2 goes through $\frac{1}{4}$ at a packing fraction of 0.54. This strongly suggests that there is a single isotropic-nematic KT transition in our system.

In order to understand the tetratic-like region we study the topological defects. In Fig. 4(a) we show a micrograph of the rods decorated with the topological defects calculated from an IDL program that we have written. We have nematiclike (π) and tetraticlike ($\pi/2$) disclinations and Ising-like domain walls. There are three length scales in this regime. The first two length scales are the between tetraticlike disclinations $L_{\pi/2} \sim 1/(\rho_{\pi/2})^{1/2}$ and the distance between the nematiclike disclinations $L_\pi \sim 1/\rho_\pi^{1/2}$ (where the ρ's are the respective disclination densities). The third length scale is the persistence length of the walls L_{wall}, which is gotten by the area and total length of the walls. We find that $L_{wall} < L_{\pi/2} < L_\pi$ ($L_{wall} \sim 7$ μm, $L_{\pi/2} \sim 41$ μm, $L_\pi > 90$ μm). In this regime the low density of free π disclinations preserves orientational order. However, the high density of meandering domain walls destroys the nematic order in favor of the tetratic. The unbound tetratic, $\pi/2$, disclinations are sufficient to destroy long-range tetratic order, but are sparse enough to give a correlation length comparable to the window for our micrographs. The decay of the correlation function g_2 will depend on both L_π and L_{wall}, while the decay of g_4 will only depend on $L_{\pi/2}$. Because in the experiment the size of a typical analyzing region, ~ 73 μm, is larger than L_{wall} and comparable to $L_{\pi/2}$, $g_2(r)$ decays quickly due to the short length of L_{wall}, while $g_4(r)$ is still observable [Fig. 4(b)].

In our system, the aspect ratio of the disks is ~ 6.4. For hard rectangles with this aspect ratio, according to Ref. [9], the system will have a continuous transition from the isotropic phase to nematic phase and the transition point is about 0.52. But for hard discorectangles [6] with the same aspect ratio [20], the system will have a first-order transition from the isotropic phase to solid phase and the transition point is about 0.78. Thus our results agree more with those of hard rectangles.

In summary, we have studied the phase diagram of a 2D system of rectangles of aspect ratio $\sim 6.4:1$. We find strong evidence for a single Kosterlitz-Thouless transition from isotropic to nematic. However, in our system we also find wall defects, and these Ising-like domain boundaries play a very important role in destroying the nematic order near the transition point. This combination of KT disclination unbinding and an Ising-like mechanism leads to a length scale where tetratic short-range order intervenes in the nematic-isotropic phase transition. We note that a tetratic phase has recently been observed in a vibrated (nonthermal) macroscopic rod system [19].

We would like to acknowledge support from NASA (Grant No. NNC04GA60G) and the MRSEC (Grant No. DMR 0213706) at Princeton.

[1] L. Onsager, Ann. N.Y. Acad. Sci. **51**, 627 (1949).
[2] P. N. Pusey, in *Liquids, Freezing and the Glass Transition*, edited by J. Hansen, D. Levesque, and J. Zinn-Justin (Elsevier, Amsterdam, 1991), Chap. 10, pp. 763–942.
[3] A. M. Somoza and P. Tarazona, Phys. Rev. Lett. **61**, 2566 (1988).
[4] J. A. C. Veerman and D. Frenkel, Phys. Rev. A **45**, 5632 (1992).
[5] A. Donev, J. Burton, F. H. Stillinger, and S. Torquato, Phys. Rev. B **73**, 054109 (2006).
[6] M. A. Bates and D. Frenkel, J. Chem. Phys. **112**, 10034 (2000).
[7] J. A. Cuesta and D. Frenkel, Phys. Rev. A **42**, 2126 (1990).
[8] K. W. Wojciechowski and D. Frenkel, Comput. Methods Sci. Technol. **10**, 235 (2004).
[9] Y. Martinez-Raton, E. Velasco, and L. Mederos, J. Chem. Phys. **122**, 064903 (2005).
[10] H. Schlacken, H.-J. Mogel, and P. Schiller, Mol. Phys. **93**, 777 (1998).
[11] T. C. Halsey, J. Phys. C **18**, 2437 (1985).
[12] A. B. D. Brown, C. G. Smith, and A. R. Rennie, Phys. Rev. E **62**, 951 (2000).
[13] P. M. Chaikin and T. Lubensky, *Principles of Condensed Matter Physics* (Cambridge University Press, Cambridge, England, 1995).
[14] For nematic liquid crystal, the free energy can be written as $F = \frac{1}{2}\int K(\nabla\theta)^2 d^2r$, so $\langle\theta(\vec{q})\theta(-\vec{q})\rangle = k_BT/(Kq^2)$, $g_{2m}(r) \simeq \exp\{-\frac{1}{2}(2m)^2\langle[\theta(r)-\theta(0)]^2\rangle\}$ and $\frac{1}{2}\langle[\theta(r)-\theta(0)]^2\rangle = \int\frac{d^2q}{(2\pi)^2}\langle\theta(\vec{q})\theta(-\vec{q})\rangle(1-e^{i\vec{q}\cdot\vec{r}})$, so we have $g_{2m}(r) \sim ar^{-2m^2k_BT/\pi K} \sim ar^{-\eta_{2m}}$, similarly $S_{2m} \sim cN^{k_BTm^2/2\pi K} \sim cN^{-\eta_{2m}/4}$.
[15] J. M. Kosterlitz and D. Thouless, J. Phys. C **6**, 1181 (1973).
[16] D. R. Nelson and J. M. Kosterlitz, Phys. Rev. Lett. **39**, 1201 (1977).
[17] D. L. Stein, Phys. Rev. B **18**, 2397 (1978).
[18] J. M. Kosterlitz, J. Phys. C **7**, 1046 (1974).
[19] S. R. V. Narayan and N. Menon, J. Stat. Mech.: Theory Exp. (2006), P01005.
[20] The definition of aspect ratio in Ref. [6] is different from our definition. In Ref. [6], the corresponding aspect ratio is $6.4-1=5.4$.